ISSN 1062-8738, Bulletin of the Russian Academy of Sciences: Physics, 2022, Vol. 86, No. 7, pp. 823–829. © Allerton Press, Inc., 2022.
Russian Text © The Author(s), 2022, published in Izvestiya Rossiiskoi Akademii Nauk, Seriya Fizicheskaya, 2022, Vol. 86, No. 7, pp. 989–996.

Effect of Regimes of Heat Transfer on the Temperature Field in Crystals during the Czochralski Process

K. A. Mitin[a], * and V. S. Berdnikov[a]

[a] *Kutateladze Institute of Thermophysics, Siberian Branch, Russian Academy of Sciences, Novosibirsk, 630090 Russia*

**e-mail: mitin@ngs.ru*

Received February 14, 2022; revised February 28, 2022; accepted March 23, 2022

Abstract—The effect uniform crystal rotation has on conjugate radiation-convective heat transfer is studied numerically in a system geometrically equal to a simplified scheme of the upper part of the growth unit in the Czochralski process. It is shown that the spatial form of convective flows becomes unstable under the action of rotation. Secondary vortices appear, substantially improving the efficiency of cooling the crystal.

DOI: 10.3103/S106287382207022X

INTRODUCTION

The Czochralski process is a common way of growing single crystals of a wide range of materials [1–3]. A single crystal is transferred from the free surface of a melt onto a seed crystal with a specified crystallographic orientation. At the initial stage of crystal growth up to a specified diameter, heat is withdrawn from the crystallization front (CF) mainly by conductivity through a single crystal to the cooled stem on which it is mounted. During the growth of a single crystal, heat is withdrawn from its lateral generatrixes mainly through convective and radiation mechanisms of heat transfer [1–8]. The relative role of conductive heat withdrawal through a single crystal and stem depends on the length of the former and the coefficients of heat conductivity of both [2, 3, 7]. The intensity of radiation–convective heat withdrawal from the crystal depends on the drop in temperature between the CF and the cold walls of the growth chamber filled with gas. The structural perfection of the resulting single crystals depends not only on the convective heat transfer at the CF, which determines its shape, but on the nonstationary fields of temperature and thermal stress inside the crystal [1, 4–8]. As the crystal grows, we must ensure the symmetry of temperature field in the crystal and the minimum temperature gradients [1–7]. The nonlinearity of problems of conjugated radiation–convective heat transfer between the crystal, melt, and environment means we must solve a great many problems at different geometries of the computational domain, which changes with the growth of the crystal. Global modeling is computer intensive, so our results from calculations were obtained in a narrow range of control parameters [4–6]. To understand the general principles of the dependence of temperature fields inside crystals on the intensity of heat withdrawal from their generatrixes and corresponding thermal stresses, it is logical to solve the problem with partial modeling [6–8]. Partial modeling by no means fully describes these processes, but it allows us to determine general trends in the behavior of the considered systems upon a change in the control parameters, either individually or in groups. The effect the rate of the crystal's uniform rotation has on the temperature fields inside the crystal at different lengths and speeds of rotation in the range of 1 to 25 rpm was studied using finite elements [9].

STATEMENT OF THE PROBLEM

Considering the axial symmetry properties of heating units used to grow single crystals in the Czochralski process, calculations were performed using a two-dimensional axial-symmetric statement. The geometry of the computational region corresponds to a simplified scheme of the upper part of the growth chamber consisting of single crystal, seed crystal, stem, walls of growth chamber, and a screen separating the melt's surface from the gas (argon) in the growth chamber. Dimensionless nonstationary system of equations of Navier–Stokes, energy and continuity to the Boussinesq approximation written in vortex variables, and the stream function, azimuthal velocity, and temperature were used to model mixed convection in gas:

$$\begin{cases} \dfrac{\partial T}{\partial t} - \dfrac{1}{Pr}\left(\dfrac{\partial^2 T}{\partial r^2} + \dfrac{1}{r}\dfrac{\partial T}{\partial r} + \dfrac{\partial^2 T}{\partial z^2}\right) + u\dfrac{\partial T}{\partial r} + \upsilon\dfrac{\partial T}{\partial z} = 0, \\ \dfrac{\partial \omega}{\partial t} - \left(\dfrac{\partial^2 \omega}{\partial r^2} + \dfrac{1}{r}\dfrac{\partial \omega}{\partial r} + \dfrac{\partial^2 \omega}{\partial z^2}\right) + u\dfrac{\partial \omega}{\partial r} + \upsilon\dfrac{\partial \omega}{\partial z} \\ + \dfrac{\omega}{r^2} - u\dfrac{\omega}{r} - \dfrac{1}{r}\dfrac{\partial W^2}{\partial z} = -Gr\dfrac{\partial T}{\partial r}, \\ \dfrac{\partial W}{\partial t} - \left(\dfrac{\partial^2 W}{\partial r^2} + \dfrac{1}{r}\dfrac{\partial W}{\partial r} + \dfrac{\partial^2 W}{\partial z^2}\right) + u\dfrac{\partial W}{\partial r} \\ + \upsilon\dfrac{\partial W}{\partial z} + \dfrac{W}{r^2} - u\dfrac{W}{r} = 0, \\ \left(\dfrac{\partial^2 \psi}{\partial r^2} + \dfrac{1}{r}\dfrac{\partial \psi}{\partial r} + \dfrac{\partial^2 \psi}{\partial z^2}\right) - \dfrac{2}{r}\dfrac{\partial \psi}{\partial r} = r \cdot \omega, \\ u = \dfrac{1}{r}\dfrac{\partial \psi}{\partial z}, \quad \upsilon = -\dfrac{1}{r}\dfrac{\partial \psi}{\partial r}, \end{cases} \tag{1}$$

where T, ω, W, ψ, u, and υ correspond to the temperature, velocity vortex, azimuthal velocity, stream function, and the radial and axial components of velocity. $Gr = (\beta g/\nu^2)\Delta T R_S^3$ is the Grashof number in dimensionless equations. Here, β is the coefficient of the volumetric expansion of gas, g is the gravitational constant, ν is the kinematic viscosity of argon, ΔT is the drop in temperature between the crystallization front and the walls of the growth chamber, and R_S is the radius of the crystal. The Prandtl number of argon $Pr = \nu/a = 0.68$, where $a = \lambda_G/\rho C_P$ is the coefficient of temperature conductivity, λ_G is the coefficient of the heat conductivity of gas, ρ is density, and C_P is the heat capacity at constant pressure. Crystal radius R_S was used as the geometric scale when reducing the equations to dimensionless form. The temperature scale corresponded to drop ΔT in temperature. The velocity scale was ν/R_S. The scale of radiation fluxes was $R_S^2/\lambda_G\Delta T$. The time scale corresponded to R_S^2/ν.

Temperature fields in a solid were calculated using the heat conductivity equation in dimensionless form on the same scale as the system of Navier–Stokes equations:

$$\frac{\partial T}{\partial t} - \frac{1}{Pr}\frac{\lambda_S}{\lambda_G}\frac{\partial^2 T}{\partial r^2} + \frac{1}{r}\frac{\partial T}{\partial r} + \frac{\partial^2 T}{\partial z^2} = 0, \tag{2}$$

where λ_G is the coefficient of the heat conductivity of a single crystal.

Radiation fluxes were calculated according to zone [10] by assuming the computational domain was limited to an isolated system of surfaces; all surfaces of the system were grey, diffusively-emitting, and diffusively-reflecting; the surfaces were split into zones, within which radiation properties and temperature can be considered constant; and the medium filling the growth chamber is diathermic. Backward ray tracing was used to determine the visibility scopes of the zones and angular coefficients were calculated that represent the fraction of radiation energy emitted by one zone that has reached another. Effective angular coefficients were calculated with known angular coefficients by assuming as many as 10 reflections of radiation flux (i.e., the fraction of radiation energy emitted by one zone and absorbed by another). The effects of the self-irradiation of a zone and self-shadowing were also considered.

The resulting radiation fluxes from the surfaces were calculated from the distribution of temperature on the surfaces of the system and the effective angular coefficients. They were then considered additions to the condition of perfect contact $-\lambda_S \left.\dfrac{\partial T}{\partial n}\right|_\Gamma = -\lambda_G \left.\dfrac{\partial T}{\partial n}\right|_\Gamma + Q$, where Q is the resulting radiation flux.

While searching for thermal stress fields, the quasi-stationary problem of thermoelasticity was solved using the thermoelastic potential of displacements [11]. Let the strain of solid thermally induced by volume expansion be specified by the displacements along axial directions u_i. We assume displacements can be expressed as $u_i = \dfrac{\partial F}{\partial i}$. Here, F is thermoelastic potential of displacement. Thermal stress fields can be determined from the distribution of the thermoelastic potential of displacements:

$$\sigma_{ij} = \frac{E}{1+\mu}\left(\frac{\partial^2 F}{\partial i \partial j} - \Delta F \delta_{ij}\right), \quad \delta = \{1 \text{ at } i = j\}. \tag{3}$$

Here, σ is the thermal stress, μ is Poisson's ratio, E is Young's modulus, Δ is the Laplacian, and δ_{ij} is the Kronecker delta. The thermoelastic potential of displacements can be found by solving Poisson's equation [11]

$$\frac{\partial^2 F}{\partial r^2} + \frac{1}{r}\frac{\partial F}{\partial r} + \frac{\partial^2 F}{\partial z^2} = \frac{1+\mu}{1-\mu}\alpha T, \tag{4}$$

where α is the coefficient of linear expansion and T is the temperature field at a specific moment in time.

The field of the thermoelastic potential of displacement was thus determined from the known temperature field distribution at a moment in time. The fields of the thermal stress components are determined from the thermoelastic potential of displacement. The von Mises equivalent stress was then determined from known distributions of the fields of thermal stress components, which are specified by the equation [11]

$$\sigma_i = \sqrt{\frac{(\sigma_{ii} - \sigma_{zz})^2 + (\sigma_{rr} - \sigma_{\varphi\varphi})^2 + (\sigma_{zz} - \sigma_{\varphi\varphi})^2 + 6\left(\sigma_{rz}^2 + \sigma_{r\varphi}^2 + \sigma_{z\varphi}^2\right)}{2}}. \tag{5}$$

The problem was solved at the boundary conditions described below. The maximum temperature in the system (1683 K) was specified on the crystallization front: $T|_{\Gamma_1} = 1$. Heat insulation, impermeability, and no-slip conditions were specified on the screen separating the melt's surface from the growth chamber: $\left.\frac{\partial T}{\partial n}\right|_{\Gamma_2} = 0$, $\psi|_{\Gamma_2} = 0$, $\omega|_{\Gamma_2} = \left.\frac{\partial V_r}{\partial z}\right|_{\Gamma_2}$. Minimum temperature in the system was maintained on the walls of growth chamber, and the impermeability and no-slip condition was specified: $T|_{\Gamma_3} = 0$, $\psi|_{\Gamma_3} = 0$, $\omega|_{\Gamma_3} = -\left.\frac{\partial V_z}{\partial r}\right|_{\Gamma_3}$. The impermeability and no-slip conditions were specified on the generatrixes of crystal and the rate of rotation and condition of perfect contact were specified by assuming radiation fluxes $\psi|_{\Gamma_4} = 0$, $\omega|_{\Gamma_4} = \left.\frac{\partial V_r}{\partial z}\right|_{\Gamma_4} - \left.\frac{\partial V_z}{\partial r}\right|_{\Gamma_4}$, $W|_{\Gamma_4} = w$, $T|_{\Gamma_{4-}} = T|_{\Gamma_{4+}}$, $-\lambda_S \left.\frac{\partial T}{\partial n}\right|_{\Gamma_{4-}} = -\lambda_G \left.\frac{\partial T}{\partial n}\right|_{\Gamma_{4+}} + Q$. The normal stress on all surfaces of the crystal is zero: $\sigma_{nn}|_{\Gamma} = 0$.

Numerical modeling was performed using finite elements on an unevenly spaced grid with 101 × 501 points consisting of triangular finite elements having the specified linear functions. Calculations were made using the heat conductivity of the crystal: $\lambda_S = 26$ W m^{-1} K^{-1}, which is characteristic of single-crystal silicon. The heat conductivity of argon was $\lambda_G = 5.83 \times 10^{-2}$ W m^{-1} K^{-1}, the temperature conductivity of gas $a = 3.74 \times 10^{-4}$ m^2 s^{-1}, the coefficient of the volumetric expansion of gas was $\beta = 6.4 \times 10^{-4}$ K^{-1}, and the kinematic viscosity of gas was $\nu = 2.54 \times 10^{-4}$ m^2 s^{-1}. The characteristics of argon at 1600 K were used [12]. Radius R_S of the crystal was 0.05 m. One dimensionless time step was 0.098 s. The emissivity of all surfaces of the system was 0.5. Poisson's ratio μ was 0.25, the crystal's coefficient of linear expansion $\alpha = 5.2 \times 10^{-6}$ K^{-1}, and Young's modulus $E = 1.59 \times 10^{-11}$ Pa.

RESULTS AND DISCUSSION

Our calculations were made in the mode of conjugated heat transfer at different combinations of the joint effect of conductive, radiation, and convective mechanisms of heat transfer. The effects of buoyancy, centrifugal forces, and their joint effect were considered during convective heat transfer. Calculations were made in the 0 to 25 rpm range of crystal rotation with Grashof number $Gr = 16000$ corresponding to drop in temperature $\Delta T = 1330$ K and set of crystal lengths $H/R_S = 2, 4, 6, 8$.

Results from calculations showed that the temperature field was nonuniform in the crystal in all regimes, so the distribution of radial and axial temperature gradients in different parts of the crystal was also nonuniform (Fig. 1). In the conductive and radiation–conductive regime (Fig. 1a), the nonuniform distribution of temperature gradients was primarily due to the complex shape of the single crystal and the notable contribution to the removal of heat from the crystal from the conductive transfer of heat through the seed crystal and stem to the cold upper part of housing.

Ignoring buoyancy but allowing for the radiative removal of heat, a stationary system of Taylor vortices arises (Fig. 1b) in the range over the crystal under the action of centrifugal force. The gas flux is slow in the near-bottom region and has virtually no effect on the field of crystal isotherms. The heat from the crystal is transferred to the environment almost in the regime of radiation-conductive heat withdrawal. As a result, we observe a drop in the total cooling of the crystal.

A stationary spatial form of convective fluxes forms under the effect of buoyancy. It consists of three vortices with the separation of the boundary layer from the generatrix of the stem at level $z = 5.5$ (Fig. 1c). A convective vortex forms with the movement of the flux in the lower part directed away from the housing walls to the base of crystal and a rising flux along its generatrixes between the generatrixes of single crystal and the cold walls of housing. The same vortex occupies part of the space over the crystal. An analogous vortex arises between the generatrixes of the stem and housing walls, partially preventing the gas warmed at the base of the crystal from moving to the upper part of growth chamber. Due to the much larger size of a convective vortex near a single crystal and more intense convective fluxes in the near-bottom region, radial gradients at the base of the crystal rise much more than the ones during convection due to centrifugal forces. Under the action of gas rising along the generatrix of a single crystal warmed at the crystallization front, the efficiency of removing heat from the lateral surface of a single crystal, and the total efficiency of cooling a single crystal warmed uniformly along its height, are reduced. The crystal in this case exists at a high temperature, the radial temperature gradients are relatively high, and the axial temperature gradients are relatively low.

With the joint effect of buoyancy and centrifugal forces, the spatial form of convective fluxes loses stability and the gas flux becomes nonstationary (Figs. 1d–1f). Secondary vortices form in the upper part of growth chamber. They travel down the stem up to the range of the seed crystal and collide with the vortex that occupies the region over the crystals and between the generatrix of the single crystal and the cold walls of the housing. Allowing for the radiative removal of heat, axial temperature gradients grow remarkably in the regime of gravitational–centrifugal convection (Figs. 1d–1f).

Figure 2 shows the temporal evolution of the velocity field in the region over a single crystal at a crystal

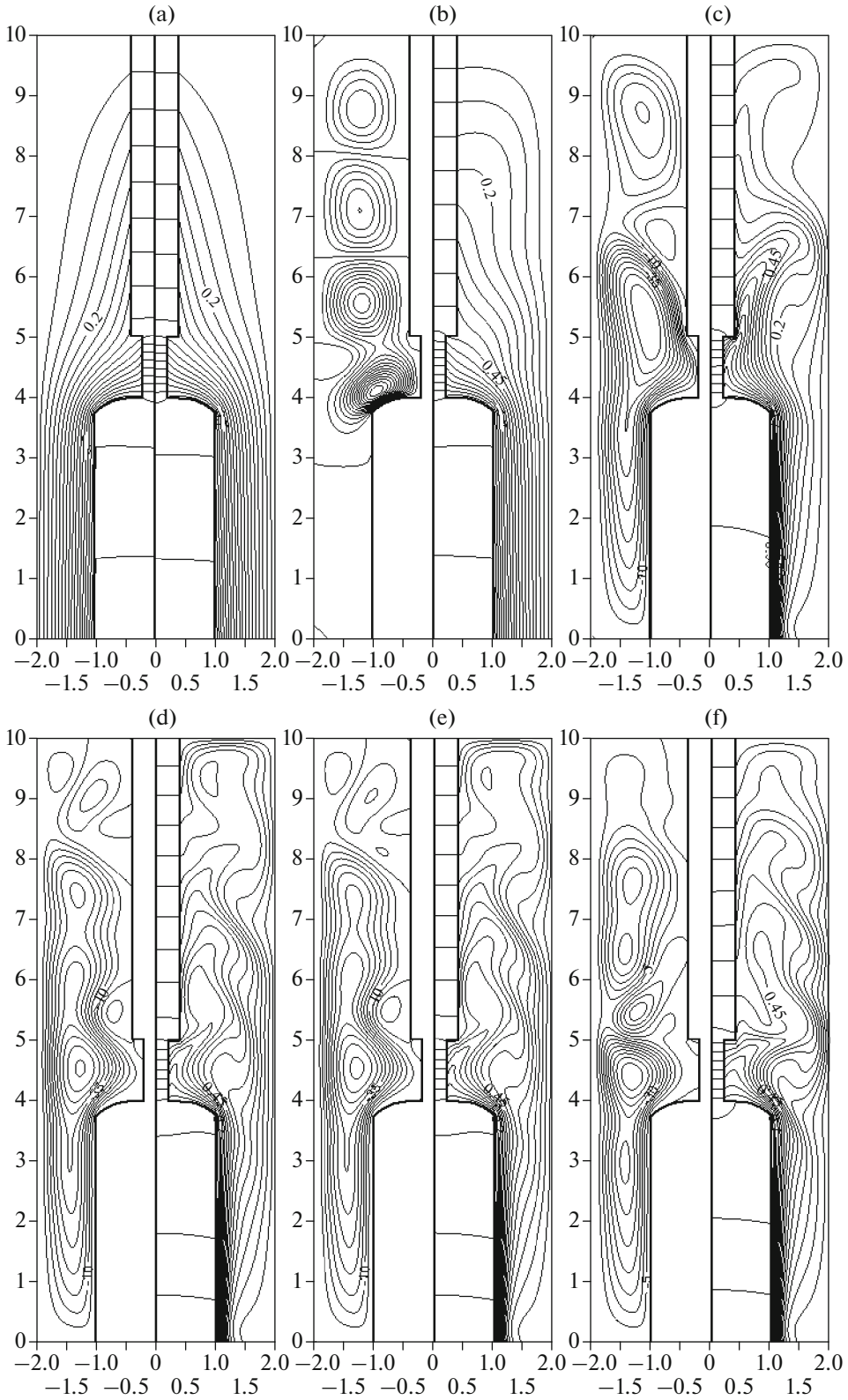

Fig. 1. Isotherms (right) and isolines (left) of the stream function at a crystal height of $H/R_S = 4$ and time $t = 200$ in different modes: (a) conductive (left) and radiation–conductive (right), (b) radiation–convective with allowance for centrifugal forces at 25 rpm, (c) radiation–convective with the allowance for buoyancy, (d) radiation–convective with allowance for centrifugal forces and buoyancy at 1 rpm, (e) radiation–convective with allowance for centrifugal forces and buoyancy at 10 rpm, and (f) radiation–convective with allowance for centrifugal forces and buoyancy at 25 rpm.

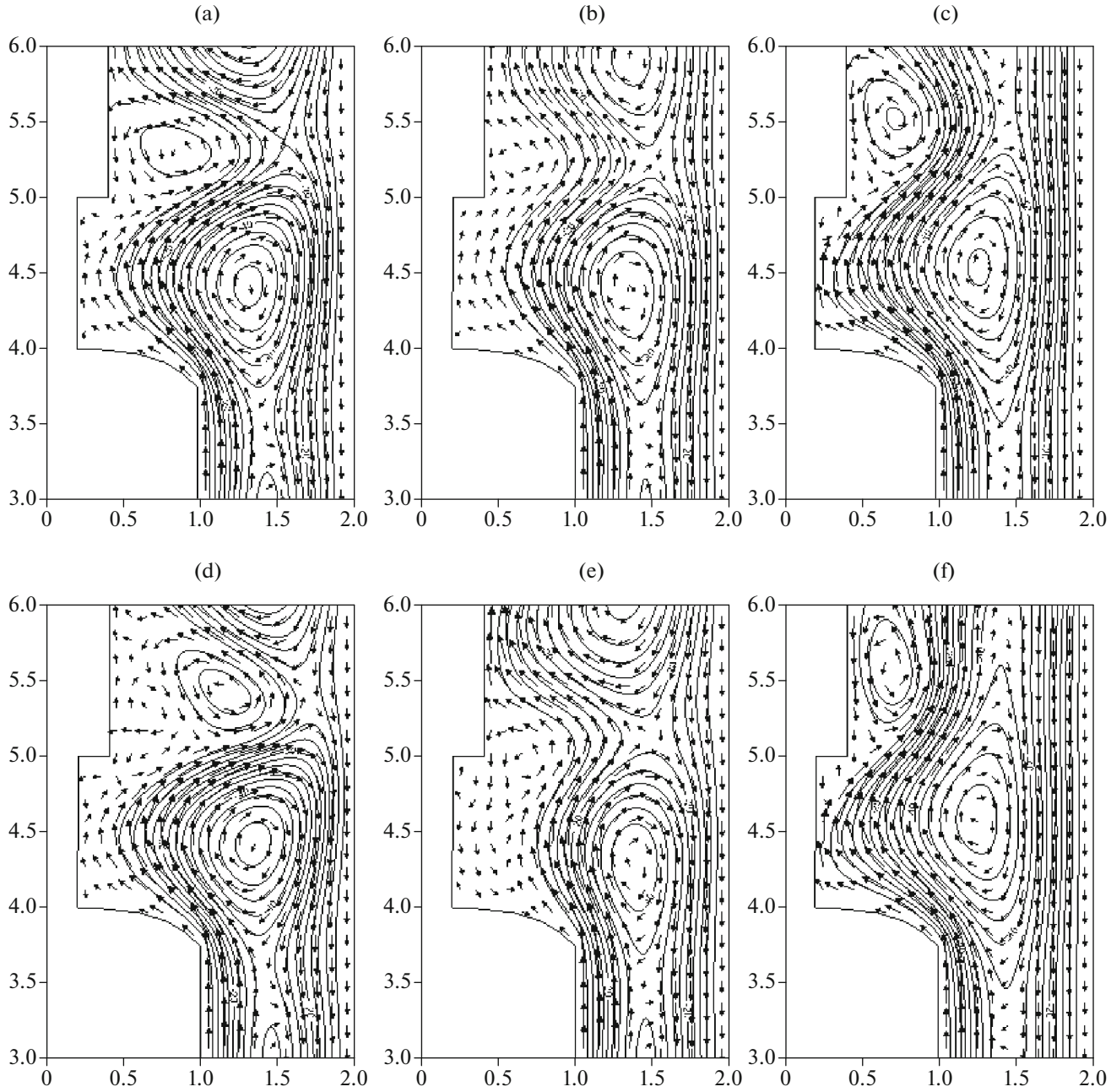

Fig. 2. Evolution of vector field of velocity and field of isolines of stream function over time, allowing for the joint effect of buoyancy and centrifugal forces, a crystal height of $H/R_S = 4$, and a 10 rpm speed of rotation at times t = (a) 35, (b) 70, (c) 105, (d) 140, (e) 175, and (f) 210.

height of $H/R_S = 4$ and a 10 rpm speed of rotation. We can the secondary vortex is pushed to the cold walls of the housing, along which it rises further when the secondary vortex collides with the one over the crystal. The warmed gas is consequently exhausted into the upper part of growth chamber, and the efficiency of cooling the single crystal falls drastically. The shape of the convective fluxes starts to stabilize as the speed of rotation grows, though it remains nonstationary. The vortex over the crystal starts to grow, partially preventing the gas heated near the base from penetrating into the upper part of the growth chamber. The efficiency of cooling of the crystal consequently falls and it is warmed more uniformly along its height (Fig. 1f).

After the flow loses its stability under the action of centrifugal forces and starts to fluctuate, the temperature field in the single crystal, seed crystal, and stem starts to oscillate (Fig. 3). Heat waves propagate in the single crystal and reach their maximum amplitude in near the top. Figure 4 shows deviations of the dimen-

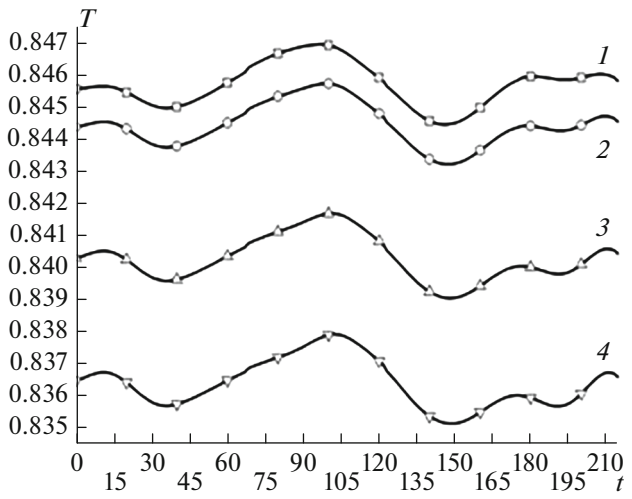

Fig. 3. Temperature reached at $z = 3.75$, allowing for the joint effect of buoyancy and centrifugal forces, a crystal height of $H/R_S = 4$, and a 10 rpm speed of rotation at points (*1*) $r = 1$; (*2*) 0.5; (*3*) 0.25; and (*4*) 0.

sional von Mises equivalent stresses at levels $z = 0.15$ m and $z = 0.05$ m, which correspond to dimensionless heights $z = 3$ and $z = 1$, from the distribution of equivalent stresses at time $t = 0$, a crystal height of $H/R_S = 4$, and a 10 rpm speed of rotation under the joint effect of buoyancy and centrifugal forces in the radiation–convective regime. We can see the thermal stresses duplicate the oscillations of the temperature field in the crystal, which are also greatest in the upper part of the crystal.

Calculations were performed at the discrete set of crystal length values $H/R_S = 2, 4, 6, 8$. At the qualitative level, patterns of the evolution of the fields of isolines of the stream function and isotherms over the upper faces of the crystals coincide. However, heat fluxes from the generatrixes of the crystals also depend on their length. Figure 5a shows the dependences of the height distributions of radial temperature gradients along the generatrixes of the crystals on their length. These dependences show the distributions of dimensionless local heat fluxes from the lateral surfaces of the crystals. Removing the heat on the generatrixes of the crystals affects the radial distributions of the radial temperature gradients in the crystals (Fig. 5b). We can see that the integral heat fluxes grow along with the length of the crystals and the area of their lateral surfaces, while the temperature gradients grow near the CF in proportion to the rise in the integral heat fluxes.

CONCLUSIONS

Finite elements were used to perform a numerical study of conjugated heat exchange in the walls of a crystal environment–growth chamber system geometrically identical to the simplified scheme of the upper part of the heating unit in the Czochralski process. Calculations were made in the conductive, radiation–conductive, and radiation–convective regimes, allowing for the effect of centrifugal forces and buoyancy. Our studies were performed at 0 to 25 rpm speeds of crystal rotation and Grashof number $Gr = 16000$ corresponding to drop in temperature $\Delta T = 1330$ K in the range of relative crystal lengths $2 \le H/R_S \le 8$. It was shown that the spatial form of convective fluxes loses stability under the effect of centrifugal forces, and fluxes of gas are transformed into fluctuating regimes at all lengths of the crystal. The evolution of gas heated near the base of a crystal to the upper part of the growth unit was observed. This resulted in the oscillating form of heat transfer from the crystal generatrixes

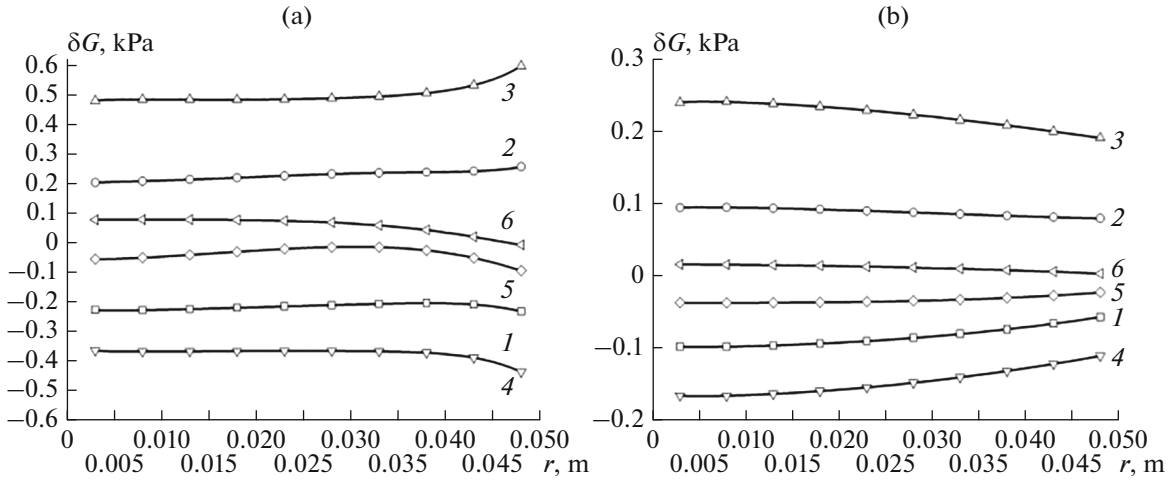

Fig. 4. Profile of deviations of von Mises equivalent stress values at $z =$ (a) 0.15 m ($z = 3$) and (b) 0.05 m ($z = 1$) on the distribution of equivalent stresses at time $t = 0$, the joint effect of buoyancy and centrifugal forces, a crystal height of $H/R_S = 4$, and a 10 rpm speed of rotation at times $t =$ (*1*) 3.4 ($t = 35$), (*2*) 6.9 (70), (*3*) 10.3 (105), (*4*) 13.8 (140), (*5*) 17.2 (175), and (*6*) 20.7 s (210).

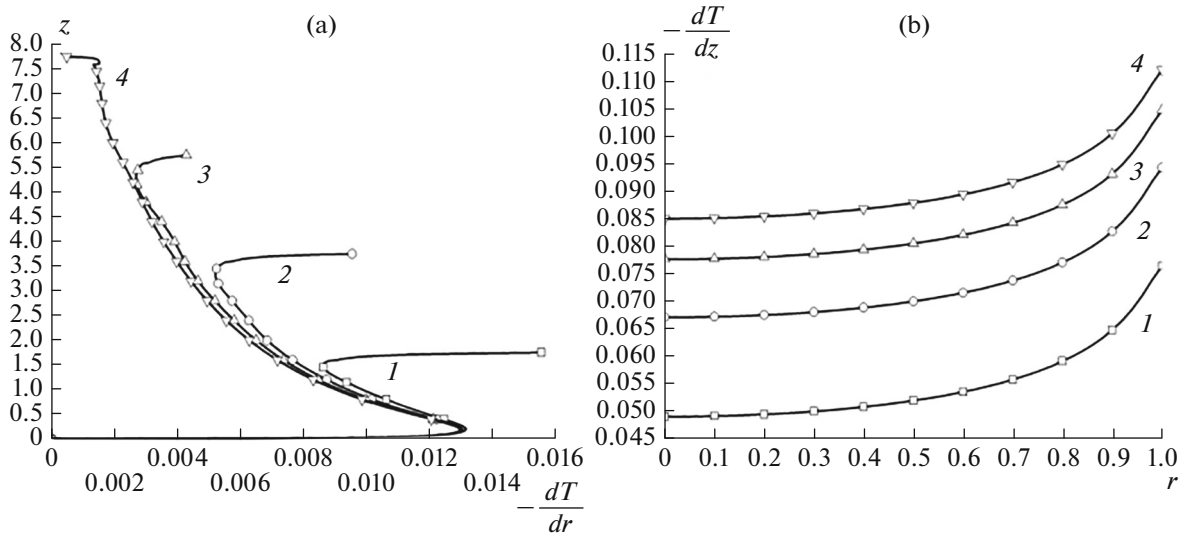

Fig. 5. Profiles of (a) radial temperature gradient in section $r = 1$ and (b) axial temperature gradient in section $z = 0.02$ in the radiation–convective mode, allowing for centrifugal forces and buoyancy at a 10 rpm speed of rotation and different heights of the crystal: $H/R_S = (1)$ 2, (2) 4, (3) 6, and (4) 8.

and the distribution of heat waves in the bulk crystal at all lengths of the crystals. Raising the speed of rotation to 25 rpm stabilized the spatial form of convective fluxes. The amplitude of oscillation of heat fluxes inside the crystal fell as the crystal grew longer.

FUNDING

This work was performed as part of a State Task for the Institute of Thermophysics, topic 0257-2021-0003 (State Registry no. 121031800213-0); and by the Russian Foundation for Basic Research, project no. 19-08-00707.

CONFLICT OF INTEREST

The authors declare they have no conflicts of interest.

REFERENCES

1. Mil'vidskii, M.G., *Poluprovodnikovye materialy v sovremennoi elektronike* (Semiconductor Materials in Modern Electronics), Moscow: Nauka, 1986.
2. Wilke, K.-Th., *Kristallzüchtund* (Crystal Growth), Berlin: Wissenschaften, 1973.
3. Goriletskii, V.I., Grinev, B.V., Zaslavskii, B.G., et al., *Rost kristallov. Galogenidy shchelochnykh metallov* (Crystal Growth: Alkali Metal Halides), Kharkov: Akta, 2002.
4. Prostomolotov, A.I., Verezub, N.A., and Il'yasov, Kh.Kh., *Izv. Vyssh. Uchebn. Zaved., Mater. Elektron. Tekh.*, 2015, vol. 18, no. 1, p. 31.
5. Verezub, N.A. and Prostomolotov, A.I., *Mech. Solids*, 2020, vol. 55, no. 5, p. 643.
6. Berdnikov, V.S. and Mitin, K.A., *Bull. Russ. Acad. Sci.: Phys.*, 2016, vol. 80, no. 1, p. 68.
7. Berdnikov, V.S., Mitin, K.A., Grigoreva, A.M., and Kleshchenok, M.S., *Bull. Russ. Acad. Sci.: Phys.*, 2017, vol. 81, no. 9, p. 1080.
8. Mitin, K.A. and Berdnikov, V.S., *J. Phys.: Conf. Ser.*, 2018, vol. 1105, 012027.
9. Soloveichik, Yu.G., Royak, M.E., and Persova, M.G., *Metod konechnykh elementov dlya resheniya skalyarnykh i vektornykh zadach* (Finite Element Method for Solving Scalar and Vector Problems), Novosibirsk: Novosib. Gos. Tekh. Univ., 2007.
10. Sparrow, E.M. and Sess, R.D., *Radiation Heat Transfer*, Washington: Hemisphere, 1962.
11. von Melan, E. and Parkus, T., *Wärmespannungen infolge Stationärer Temperaturfelder* (Thermal Stresses due to Stationary Temperature Fields), Vienna: Springer, 1953.
12. Vargaftik, N.B., *Spravochnik po teplofizicheskim svoistvam gazov i zhidkostei* (Handbook of Thermophysical Properties of Gases and Liquids), Moscow: Nauka, 1972.

Translated by A. Muravev